Available online at www.sciencedirect.com
SCIENCE DIRECT®
Journal of Sound and Vibration 278 (2004) 611–635
JOURNAL OF SOUND AND VIBRATION
www.elsevier.com/locate/jsvi

The non-stationary freefield response for a moving load with a random amplitude

G. Lombaert[a,*], G. Degrande[a], D. Clouteau[b]

[a] *Department of Civil Engineering, Katholieke Universiteit Leuven, Kasteelpark Arenberg 40, B-3001 Leuven, Belgium*
[b] *Laboratoire de Mécanique des Sols, Ecole Centrale de Paris, Structures et Matériaux, F-92295 Châtenay-Malabry, France*

Received 13 December 2002; accepted 13 October 2003

Abstract

This paper presents a stochastic solution procedure for the calculation of the non-stationary freefield response due to a moving load with a random amplitude. In this case, a non-stationary autocorrelation function and a time-dependent spectral density are required to characterize the response at a fixed point in the freefield. The non-stationary solution is derived from the solution in the case of a moving load with a deterministic amplitude. It is shown how the deterministic solution can be calculated in an efficient way by means of integral transformation methods if the problem geometry exhibits a translational invariance in the direction of the moving load. A key ingredient is the transfer function between the source and the receiver that represents the fundamental response in the freefield due to an impulse load at a fixed location. The solution in the case of a moving load with a random amplitude is formulated in terms of the double forward Fourier transform of the non-stationary autocorrelation function. The solution procedure is illustrated with an example where the non-stationary autocorrelation function and the time-dependent standard deviation of the freefield response are computed for a moving harmonic load with a random phase shift. The results are compared with the response in the deterministic case.

1. Introduction

Ground-borne traffic-induced vibrations in buildings are a matter of growing environmental concern. Vibrations induced by road traffic are mainly due to heavy vehicles that pass at relatively

*Corresponding author. Fax: +32-16-32-19-88.
E-mail addresses: geert.dugrande@bwk.kuleuven.ac.be (G. Lombaert), clouteau@mss.ecp.fr (D. Clouteau).
URL: http://www.kuleuven.ac.be/bwm.

0022-460X/$ - see front matter © 2003 Elsevier Ltd. All rights reserved.
doi:10.1016/j.jsv.2003.10.045

high speed on a road with an uneven surface. The growing traffic volume, the higher vehicle speeds and the larger axle loads are generally considered to be responsible for the increasing nuisance due to road traffic-induced vibrations. Considering rail traffic, vibration nuisance is related to increasing train speeds and larger freight loads.

In various prediction models for traffic-induced vibrations, solution procedures are presented that allow for the computation of the response to deterministic moving loads. These procedures are based on a Galilean transformation to the moving frame of reference or on the application of the Betti–Rayleigh reciprocal theorem [1]. An extensive survey of calculation methods for solids or structures under moving loads is given by Frýba [2].

Müller [3] and Müller and Huber [4] have solved the problem of a layered visco-elastic half-space subjected to a constant and a transient moving load in the frequency–wavenumber domain (k_x, k_y, z, ω). Similarly, de Barros and Luco [5,6] have studied the steady state response of a layered visco-elastic half-space due to a constant moving load. Grundmann et al. [7] have considered the same problem and applied an additional wavelet transform on the response of the layered half-space in the frequency–wavenumber domain in order to efficiently evaluate the inverse wavenumber domain transformations.

For a 3D problem geometry that is invariant in the direction $\mathbf{e}_y$ of the moving load, Aubry et al. [8], Clouteau [9] and Clouteau et al. [10] derive a solution in the frequency–wavenumber domain (x, k_y, z, ω). Hardy [11], Madshus and Kaynia [12] and Degrande and Lombaert [13] show how this formulation results in a graphical representation that is useful for the study of the generation of waves by moving loads.

Road and railway unevenness are often described as a stationary random process by means of the power spectral density (PSD) function in terms of the wavenumber $k_y = 2\pi/\lambda_y$ along the road [14,15] or the railway track. Whereas the axle loads of the vehicles represent a stationary random process as well, this is not the case for the vibrations observed in the freefield. This is due to the fact that, for a receiver at a fixed position in the freefield, the vibration level depends on the position y of the vehicle along the road or on the time t and is therefore a non-stationary random process. As a result, non-stationary stochastic methods are required for the statistical characterization of the response.

Stationary stochastic methods can only be applied if the motion of the axle loads is neglected [16,17]. Alternatively, Sun and Greenberg [18] have proposed to consider the stationary problem of the response in a frame of reference that moves with the source.

In the following, the Wigner–Ville method [19] is applied to calculate the time-dependent statistical characteristics of the freefield response for a moving load with a random amplitude [20]. First, the deterministic solution procedure is briefly recapitulated [21]. The dynamic Betti–Rayleigh reciprocity theorem is used to compute the response for a moving load from the fundamental response for an impulse load at a fixed position. Next, it is shown how these deterministic results are used to calculate the double power spectral density and the Wigner–Ville distribution. Finally, the solution procedure is illustrated for the case of a moving harmonic load with a random phase shift. The time-dependent standard deviation of the freefield response is calculated for two source speeds.

This solution method has been developed as a part of a numerical model for the freefield vibrations induced by road [21] and railway [22–24] traffic. The model has been extensively validated by means of in situ measurements [22–26].

2. The response for a set of deterministic moving loads

2.1. Introduction

The response of a road–soil or a railway track–soil system to a moving load has recently received considerable attention in the literature [10–13,21]. The solution of this problem enables the study of the dynamic road or railway track response and the vibrations produced in the freefield.

In the case where the problem geometry is invariant in the direction of the moving load, the dynamic Betti–Rayleigh reciprocal theorem can be used to compute the response for a moving load from the solution for an impulse load at a fixed position [1,10,13,21], which is considered as a source–receiver transfer function.

In the following, it is first shown how the track–soil transfer function can be calculated in an efficient way by means of integral transformation methods. Next, the transfer function is used to calculate the response in the case of a time-dependent moving load. Finally, the special case of a harmonic moving load is considered.

2.2. The response for a fixed impulse load

The calculation of the track–soil transfer function requires the solution of the equations of motion of the coupled track–soil system for an impulse load at a fixed position (Fig. 1). In the case where the track is invariant in the longitudinal direction $\mathbf{e}_y$, this solution can be efficiently obtained in the frequency–wavenumber domain (x, k_y, z, ω) [13,21].

The double forward Fourier transformation from the spatial domain (x, y, z, t) to the frequency–wavenumber domain is defined as follows. First, the Fourier transform of $f(x, y, z, t)$ with respect to the time t, denoted as $\hat{f}(x, y, z, \omega)$, is obtained by the following transformation

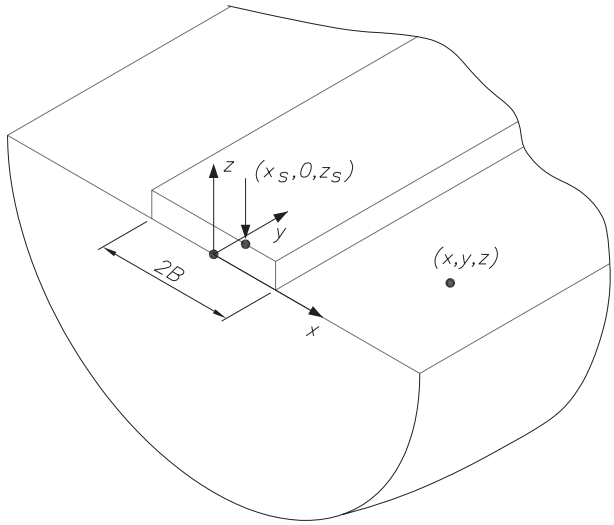

Fig. 1. The freefield response for an impulse load at a fixed position $\{x_S, 0, z_S\}^{\mathrm{T}}$ along the source path.

from the time t to the circular frequency ω:

$$\hat{f}(x,y,z,\omega) = \int_{-\infty}^{+\infty} f(x,y,z,t)\exp(-\mathrm{i}\omega t)\,\mathrm{d}t. \tag{1}$$

Next, the forward Fourier transform of $\hat{f}(x,y,z,\omega)$ with respect to y, denoted as $\tilde{f}(x,k_y,z,\omega)$, is obtained by a transformation from the horizontal co-ordinate y to the horizontal wavenumber k_y:

$$\tilde{f}(x,k_y,z,\omega) = \int_{-\infty}^{+\infty} \hat{f}(x,y,z,\omega)\exp(+\mathrm{i}k_y y)\,\mathrm{d}y. \tag{2}$$

The numerical models currently used to predict road or railway traffic-induced vibrations are often based on the model of an elastic beam, coupled to a horizontally layered half-space. In the case of railway traffic, other elements are coupled to the beam to model the rails, the sleepers and the railway pads. In both the case of road or railway traffic, however, the equations of motion in the frequency–wavenumber domain can be formulated as follows:

$$[\tilde{\mathbf{K}}_r + \tilde{\mathbf{K}}_s]\tilde{\mathbf{u}}_r = \tilde{\mathbf{f}}_r, \tag{3}$$

where $\tilde{\mathbf{K}}_r$ is the dynamic impedance of the road or the railway track, $\tilde{\mathbf{K}}_s$ denotes the soil impedance, $\tilde{\mathbf{u}}_r$ is the vector that collects the displacements of the road or the railway track and $\tilde{\mathbf{f}}_r$ contains the contribution from the fixed impulse load. In the present paper, a road model is considered, where the road is represented by a beam which longitudinal bending and torsional deformations are accounted for. In this case, the vector $\tilde{\mathbf{u}}_r$ contains the vertical displacement $\tilde{u}_{cz}$ of the section's centre of gravity and the rotation $\tilde{\beta}_{cy}$ about this centre.

This results in the following decomposition of the road displacements in the frequency–wavenumber domain:

$$\tilde{u}_{rz}(x,k_y,\omega) = \tilde{u}_{cz}(k_y,\omega) + x\tilde{\beta}_{cy}(k_y,\omega) = \boldsymbol{\phi}_r(x)\tilde{\mathbf{u}}_r. \tag{4}$$

The vector $\boldsymbol{\phi}_r = \{1, x\}^{\mathrm{T}}$ collects the displacement modes of the rigid cross-section. The displacements $\tilde{\mathbf{u}}_r$ can also be considered as the unknown modal co-ordinates $\tilde{\boldsymbol{\alpha}}$ of the road's deformation modes.

The road impedance matrix $\tilde{\mathbf{K}}_r$ contains the contribution from the road's longitudinal bending and torsional stiffness:

$$\tilde{\mathbf{K}}_r = \begin{bmatrix} EI_x k_y^4 - \rho A\omega^2 & 0 \\ 0 & GCk_y^2 - \rho I_p\omega^2 \end{bmatrix}, \tag{5}$$

where A is the road's cross-section, I_x the moment of inertia with respect to x, C the torsional moment of inertia and I_p the polar moment of inertia; E is Young's modulus, G the shear modulus and ρ the density of the road.

The contribution of the soil to the impedance of the coupled road–soil system follows from the equilibrium at the road–soil interface Σ and is calculated as follows:

$$\tilde{\mathbf{K}}_s = \int_{\Sigma} \boldsymbol{\phi}_r \tilde{t}_{sz}(\tilde{\boldsymbol{\phi}}_s)\,\mathrm{d}\Gamma, \tag{6}$$

where $\tilde{t}_{sz}(\tilde{\boldsymbol{\phi}}_s)$ is the frequency–wavenumber domain representation of $t_{sz}(\boldsymbol{\phi}_s)$, the vertical component of the soil tractions $\mathbf{t}_s = \sigma_s\mathbf{n}$ on a boundary with a unit outward normal $\mathbf{n}$ for the wave fields $\tilde{\boldsymbol{\phi}}_s$ scattered by the road's deformation modes $\boldsymbol{\phi}_r$.

A boundary element method is used to calculate the soil tractions $\tilde{t}_{sz}(\tilde{\boldsymbol{\phi}}_s)$ at the road–soil interface [8,21]. The boundary element formulation is based on the formulation of the boundary integral equations in the frequency–wavenumber domain, using the Green's functions of a horizontally layered elastic half-space [27–29].

The force vector $\tilde{\mathbf{f}}_r$ contains the contribution of the impulse load applied in the point $(x_S, 0, z_S)$ of the road–soil interface Σ and is equal to $\{1, x_S\}^{\mathrm{T}}$ in the present case.

The solution of the system of Eq. (3) gives the complex participation factors $\tilde{\boldsymbol{\alpha}}$. The soil tractions $\tilde{t}_{sz}(\tilde{\mathbf{u}}_s)$ at the road–soil interface are calculated from the participation factors as $\tilde{t}_{sz}(\tilde{\boldsymbol{\phi}}_s)\tilde{\boldsymbol{\alpha}}$.

The reciprocity theorem is used for the calculation of the road–soil transfer function $\tilde{h}_{zi}(\xi_1, k_y, \xi_3, \omega)$ from the soil tractions $\tilde{t}_{sz}(\tilde{\boldsymbol{\phi}}_s)\tilde{\boldsymbol{\alpha}}$:

$$\tilde{h}_{zi}(\xi_1, k_y, \xi_3, \omega) = \int_{\Sigma} \tilde{u}^G_{zi}(\xi_1 - x, k_y, \xi_3, \omega)\tilde{t}_{sz}(x, k_y, z = 0, \omega)\,\mathrm{d}\Gamma, \tag{7}$$

where $\tilde{u}^G_{zi}(\xi_1, k_y, \xi_3, \omega)$ denotes the Green's function that represents the fundamental solution for the displacement component i due to a vertical impulse load. A double inverse Fourier transformation from the frequency–wavenumber domain to the time-spatial domain results in the transfer function $h_{zi}(\xi_1, \xi_2, \xi_3, t)$.

2.3. An arbitrary time-dependent moving load

The dynamic Betti–Rayleigh reciprocal theorem specifies the relations between the field variables in two elastodynamic states. In the unknown first state, a vertical moving load $\rho b_j(\mathbf{x}, t) = \delta(\mathbf{x} - \mathbf{x}_{Sk}(t))g_k(t)\delta_{zj}$ is considered, where $\mathbf{x}_{Sk}(t)$ denotes the time-dependent position $\{x_S, y_k + vt, z_S\}^{\mathrm{T}}$ of the load and $g_k(t)$ the time history. The second state is the case where an impulse load is applied at the point $\{x_S, 0, z_S\}^{\mathrm{T}}$ (Fig. 1).

In the case where the problem geometry is invariant in the direction $\mathbf{e}_y$ of the moving load, the following expression can be derived for the unknown response $u_{si}(x, y, z, t)$:

$$u_{si}(x, y, z, t) = \int_{-\infty}^{t} g_k(\tau)h_{zi}(x, y - y_k - v\tau, z, t - \tau)\,\mathrm{d}\tau. \tag{8}$$

The co-ordinates $\{x, y - y_k - v\tau, z\}^{\mathrm{T}}$ in the argument of the transfer function correspond to a receiver that moves in the opposite direction of the moving source. The motion of the source is replaced by an equivalent motion of the receiver.

In Section 2.2, it has been shown how the transfer function can be efficiently computed by means of a transformation from the spatial-time domain (x, y, z, t) to the frequency–wavenumber domain (x, k_y, z, ω). It is therefore advantageous to apply a similar double forward Fourier transformation to Eq. (8):

$$\tilde{u}_{si}(x, k_y, z, \omega) = \int_{-\infty}^{+\infty} \int_{-\infty}^{+\infty} g_k(\tau)\hat{h}_{zi}(x, y - y_k - v\tau, z, \omega)\exp(-\mathrm{i}\omega\tau)\,\mathrm{d}\tau\exp(+\mathrm{i}k_y y)\,\mathrm{d}y. \tag{9}$$

This equation can be further elaborated, yielding the following solution in the frequency–wavenumber domain [30]:

$$\tilde{u}_{si}(x, k_y, z, \omega) = \hat{g}_k(\omega - k_y v)\tilde{h}_{zi}(x, k_y, z, \omega)\exp(+\mathrm{i}k_y y_k). \tag{10}$$

The response is computed as the product of the transfer function and the frequency content of the source, provided that the latter is shifted by $k_y v$. For a limiting small velocity v, this shift tends to zero and the solution for the case of a load at a fixed position is recovered.

The frequency content $\hat{u}_{si}(x, y, z, \omega)$ of the response can be computed as the inverse wavenumber domain transformation:

$$\hat{u}_{si}(x, y, z, \omega) = \frac{1}{2\pi} \int_{-\infty}^{+\infty} \hat{g}_k(\omega - k_y v) \tilde{h}_{zi}(x, k_y, z, \omega) \exp[-\mathrm{i} k_y (y - y_k)] \, \mathrm{d}k_y. \tag{11}$$

A change of variables according to $k_y = (\omega - \tilde{\omega})/v$ moves the frequency shift from the frequency content of the moving load to the wavenumber content of the transfer function:

$$\hat{u}_{si}(x, y, z, \omega) = \frac{1}{2\pi v} \int_{-\infty}^{+\infty} \hat{g}_k(\tilde{\omega}) \tilde{h}_{zi}\left(x, \frac{\omega - \tilde{\omega}}{v}, z, \omega\right) \exp\left[-\mathrm{i}\left(\frac{\omega - \tilde{\omega}}{v}\right)(y - y_k)\right] \mathrm{d}\tilde{\omega}. \tag{12}$$

The frequency content $\hat{g}_k(\tilde{\omega})$ of the load and the displacement $\hat{u}_{si}(x, y, z, \omega)$ are coupled through the wavenumber at which the transfer function is evaluated. For a limiting large velocity v, the wavenumber $k_y = (\omega - \tilde{\omega})/v$ tends to zero and the solution for the 2D case of a line load along the path of the moving source is obtained.

The response in the time domain is finally obtained as the inverse Fourier transform of Eq. (12):

$$u_{si}(x, y, z, t) = \frac{1}{2\pi} \int_{-\infty}^{+\infty} \hat{u}_{si}(x, y, z, \omega) \exp(+\mathrm{i}\omega t) \, \mathrm{d}\omega. \tag{13}$$

The response for a set of moving axle loads is found from superposition (summation on k).

2.4. A harmonic moving load

In the case of a harmonic moving load, the time history $g(t)$ is equal to $P \exp(+\mathrm{i}\tilde{\omega}_S t)$ and the frequency content $\hat{g}(\tilde{\omega})$ equals $2\pi P \delta(\tilde{\omega} - \tilde{\omega}_S)$. The introduction of $\hat{g}(\tilde{\omega})$ in Eq. (12) results in the following expression for the freefield displacements:

$$\hat{u}_{si}(x, y, z, \omega) = \frac{1}{v} \tilde{h}_{zi}\left(x, \frac{\omega - \tilde{\omega}_S}{v}, z, \omega\right) \exp\left[-\mathrm{i}\left(\frac{\omega - \tilde{\omega}_S}{v}\right) y\right]. \tag{14}$$

This equation shows that the response at a circular frequency ω for a harmonic moving load is proportional to the transfer function $\tilde{h}_{zi}(x, k_y, z, \omega)$, where the horizontal wavenumber k_y is evaluated at $(\omega - \tilde{\omega}_S)/v$.

The relations $k_y = (\omega - \tilde{\omega}_S)/v$ and $C_y = \omega/k_y$, with C_y the phase velocity in the y direction, are used to write the circular frequency ω at the receiver as $\omega = \tilde{\omega}_S/(1 - v/C_y)$. When the source approaches, the response is mainly composed of waves that travel in the positive y direction and the circular frequency $\tilde{\omega}_S$ emitted at the source results in higher frequencies $\tilde{\omega}_S/(1 - v/C_y)$ at the receiver. When the source recedes, the response is mainly composed of waves that travel in the negative y direction with a negative phase velocity C_y and the circular frequency $\tilde{\omega}_S$ emitted at the source results in lower frequencies at the receiver. This phenomenon is known as the Doppler effect.

2.5. Numerical examples

In the following numerical examples, the freefield response is computed for the case of a harmonic load moving on a road supported by a homogeneous half-space.

The road is modelled as a beam with a rigid cross-section supported by a horizontally layered half-space. Both the road's longitudinal bending and torsional deformations are taken into account [21].

The road has a width $2B = 3$ m, a bending stiffness $EI = 1.611 \times 10^8$ N m^2, a mass per unit length $\rho A = 3.282 \times 10^3$ kg/m, a torsional stiffness $\rho I_p = 2.603 \times 10^3$ kg m and a torsional moment of inertia $GC = 2.094 \times 10^8$ N m^2. The soil is modelled as a homogeneous half-space with a density $\rho = 1800$ kg/m^3, a shear (S-) wave velocity $C_s = 150$ m/s, a dilatational (P-) wave velocity $C_p = 300$ m/s and a hysteretic material damping ratio $\beta = 0.025$ in shear and volumetric deformation. The ratio s of the body wave velocities C_s and C_p equals 0.5 for $\nu = 1/3$. The Rayleigh or surface (R-) wave velocity $C_R = 140$ m/s and is slightly lower than the S-wave velocity. The S-wave velocity C_s of the supporting half-space is used to define the dimensionless wavenumber $\bar{k}_y = k_y C_s/\omega$.

The dynamic road–soil interaction problem is solved by means of a substructure method in the frequency–wavenumber domain (x, k_y, z, ω) [8,21]. The soil's impedance is calculated by means of a boundary element method, that is based on the Green's functions of the horizontally layered half-space [28,29,31–33]. The road–soil transfer functions are calculated at the soil's free surface at distances x equal to 8 and 40 m from the road, for frequencies between 0.5 and 50 Hz, with a step $\Delta f = 0.50$ Hz, and dimensionless wavenumbers $\bar{k}_y = k_y C_s/\omega$ between 0 and 1.50, with a step $\Delta \bar{k}_y = 0.01$ [30].

The freefield displacements are calculated for a vertical harmonic load with a time history $g(t) = \cos(\tilde{\omega}_S t) = 0.50[\exp(+\mathrm{i}\tilde{\omega}_S t) + \exp(-\mathrm{i}\tilde{\omega}_S t)]$ with $\tilde{\omega}_S = 2\pi 15$ rad/s and an initial position $y_k = 0$. Two source speeds $v = 20$ m/s and $v = 60$ m/s are considered.

It can be shown that, for load speeds v that are low compared to the Rayleigh wave velocity C_R, the contribution of the term $0.50\exp(-\mathrm{i}\tilde{\omega}_S t)$ to the frequency content $\hat{u}_{si}(x, y, z, \omega)$ at positive circular frequencies ω can be neglected compared to the contribution of the term $0.50\exp(+\mathrm{i}\tilde{\omega}_S t)$ [30]. The opposite is true for negative ω.

The frequency content of the response (Fig. 2a) is calculated upto 50 Hz by means of Eq. (14), with a step $\Delta f = 0.0244$ Hz ($N = 2048$), corresponding to a period $T = 40.96$ s and a time step $\Delta t = 0.01$ s. Each signal is denoted by a label `FFij`, where `FF` denotes the freefield, `i` the x-coordinate of the receiver and `j` the component $\mathbf{e}_x$, $\mathbf{e}_y$ or $\mathbf{e}_z$.

The frequency content of the x-component does not show sharp peaks. From Eq. (14), it follows that the response is mainly situated in a frequency band $[\tilde{\omega}_S/(1 + v/C_R), \tilde{\omega}_S/(1 - v/C_R)]$ with a width $\tilde{\omega}_S[2v/C_R(1 - (v/C_R)^2)]$ that is proportional to $\tilde{\omega}_S$. For small speeds v with respect to C_R, this bandwidth is proportional to v as $2\tilde{\omega}_S v/C_R$.

The frequency content of the y-component presents 4 sharp peaks. These peaks correspond to the contribution of the P-, S- and R-waves in the y direction during the approaching and the receding of the source. For a wave with a velocity C, the location of the peaks in the frequency domain can be estimated as $\tilde{\omega}/(1 \pm v/C)$. The P-wave velocity C_p is much larger than the R- and S-wave velocities C_s and C_R; the peaks that correspond to this type of wave are located near $\tilde{\omega}_S$. C_R is close to C_s and the contributions of these waves at both other peaks in Fig. 2b are not

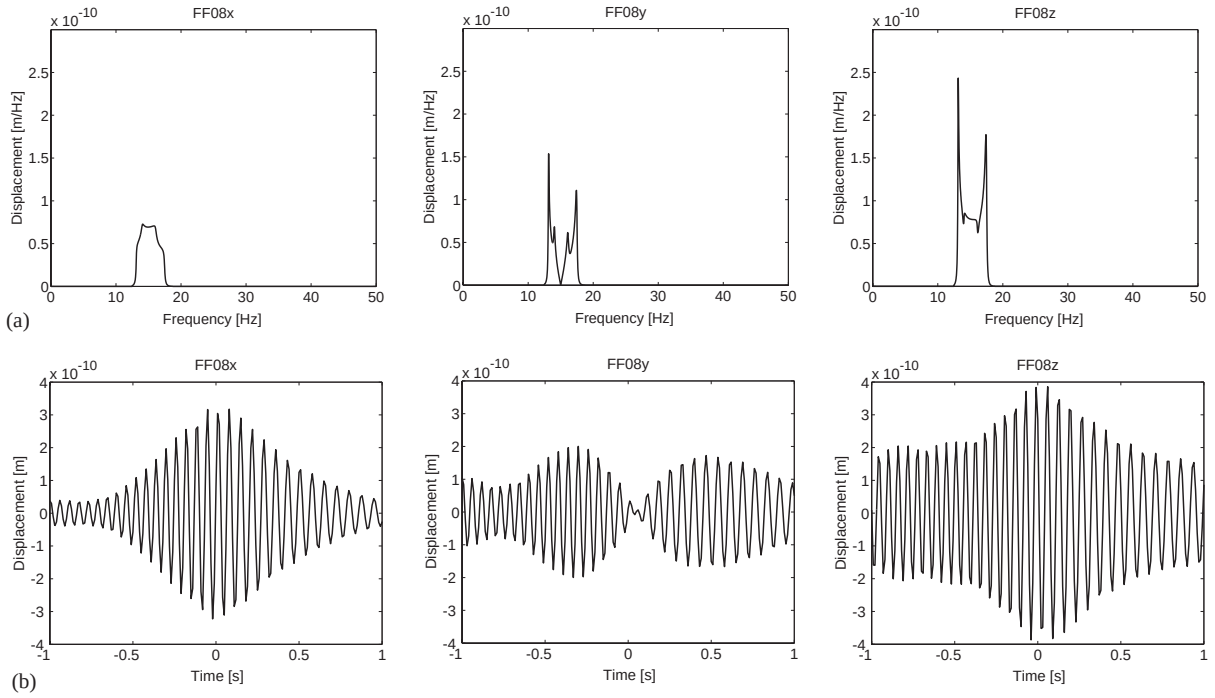

Fig. 2. (a) Frequency content and (b) time history of the freefield displacement at $x = 8$ m for a moving harmonic load with a frequency $\tilde{\omega}_S = 2\pi 15$ Hz and a speed $v = 20$ m/s.

distinguishable. The contribution at $\omega = \tilde{\omega}_S$ is zero as, according to Eq. (14), $k_y = 0$ at this frequency and waves propagate in the x direction only.

The frequency content of the vertical component of the displacements is dominated by the contribution of the S- and R-waves.

The time histories in Fig. 2b are calculated by means of a FFT algorithm. The response is nearly periodic with a period $T = 2\pi/\omega_S$. Due to the Doppler effect, the period is smaller during the approaching of the source and larger during the receding. The amplitude is approximately inversely proportional to the distance between the source and the receiver. The interference between P-, S- and R-waves influences the time history of the horizontal components. The x- and z-component have the same order of magnitude. At $t = 0$, the source and the receiver are at the same y-co-ordinate and the x- and z-component are maximal, while the y-component vanishes.

Fig. 3 shows similar results for the response at 40 m from the centre of the road. The contribution of the body and surface waves in the y direction no longer dominates the frequency content at a large distance x. The duration of the transient signals is larger.

Fig. 4 shows similar results for a load speed $v = 60$ m/s. Eq. (14) indicates that, for a larger load speed v, the frequency content is situated in a wider frequency range. As according to Eq. (14), the frequency content of the response is inversely proportional to the load speed v and the modulus of the response in Fig. 4a at a circular frequency $\omega = \tilde{\omega}_S$ is exactly one third of the value in Fig. 2b. Fig. 4b shows the time history of the freefield displacements. Due to the larger speed of the source,

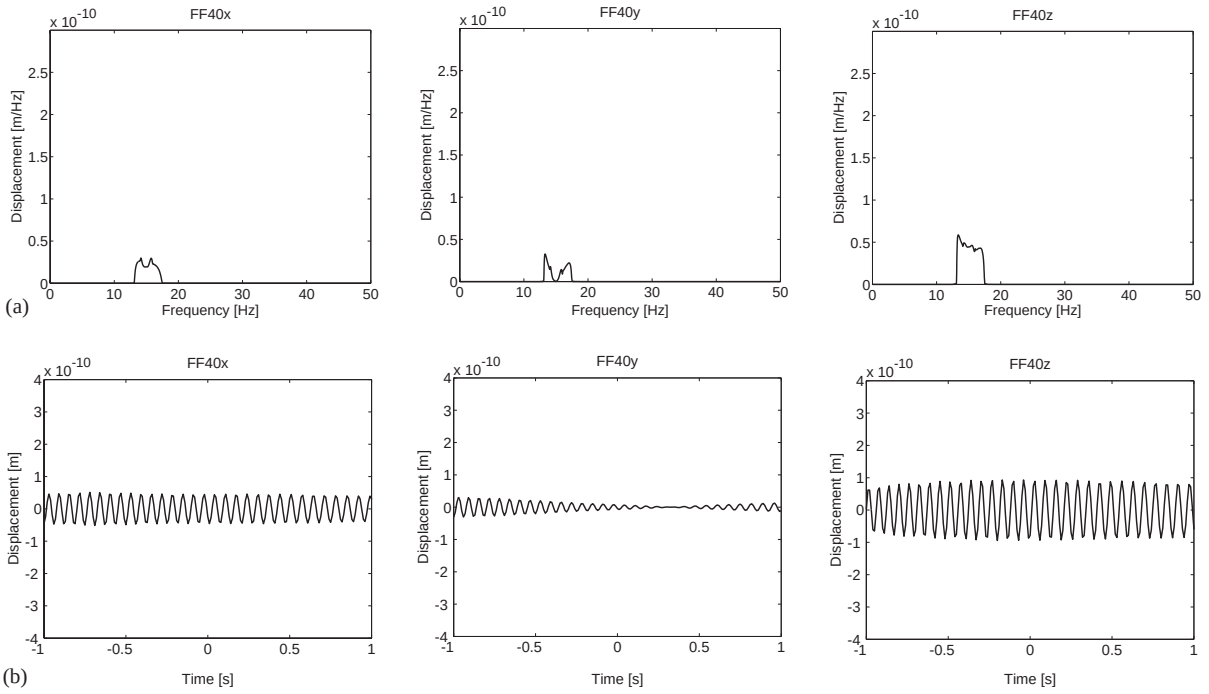

Fig. 3. (a) Frequency content and (b) time history of the freefield displacement at $x = 40$ m for a moving harmonic load with a frequency $\tilde{\omega}_S = 2\pi 15$ Hz and a speed $v = 20$ m/s.

the duration of the passage is shorter and the Doppler effect is more pronounced. The peak displacement has the same order of magnitude as in the case where $v = 20$ m/s.

Fig. 5 shows similar results for the response at 40 m from the centre of the road. The frequency content shows no peaks and almost has a uniform value in the frequency band $[\tilde{\omega}/(1 + v/C_R), \tilde{\omega}/(1 - v/C_R)]$. The transient signal has a smaller duration than in Fig. 3c, whereas the peak displacement has the same order of magnitude.

The foregoing results indicate that, if the speed v of the load is low with respect to the wave velocities in the soil, the peak response is mainly determined by the distance between the source and the receiver.

3. The response for a set of random moving loads

3.1. Introduction

The previous examples show how the vibration levels vary as the deterministic moving load passes a receiver. Even in the case where the time history of the load is a stationary random process, the motion of the load results in a non-stationary response. The statistical properties are time-dependent and can be computed using non-stationary stochastic methods.

In the following, the Wigner–Ville method is used to characterize the time-dependent statistical properties of the response due to a random moving load. First, the definitions of the local

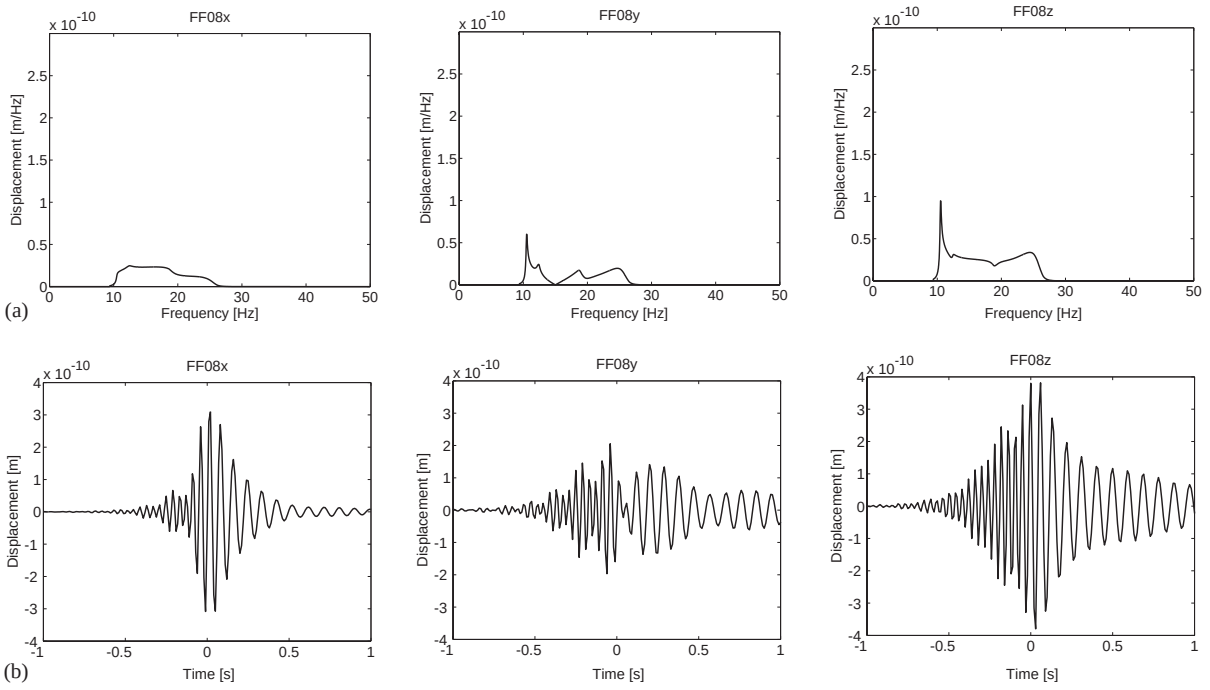

Fig. 4. (a) Frequency content and (b) time history of the freefield displacement at $x = 8$ m for a moving harmonic load with a frequency $\tilde{\omega}_S = 2\pi 15$ Hz and a speed $v = 60$ m/s.

autocorrelation function and the double spectral density are briefly recapitulated. Next, the deterministic solution is used to compute the double spectral density of the response due to a random moving load. Finally, the special case of a random harmonic moving load is considered and the solution procedure is illustrated.

3.2. The Wigner–Ville method

The Wigner–Ville method [19] is based on the work of Wigner [34] in the field of quantum mechanics and the work of Ville [35] in signal theory. This method offers an alternative approach for the calculation of the statistical characteristics of non-stationary processes. It is based on the use of an instantaneous autocorrelation function, defined as follows [19] for a random process $x(t)$:

$$R_x(t_0, t_1) = E\left[x\left(t_0 - \frac{t_1}{2}\right)x\left(t_0 + \frac{t_1}{2}\right)\right], \tag{15}$$

where t_0 represents the absolute time and t_1 is the separation time. The latter has a similar role as the argument τ in the definition of the stationary autocorrelation function $R_x(\tau) = E[x(t)x(t+\tau)]$. By definition, the evaluation of the instantaneous autocorrelation function $R_x(t_0, t_1)$ at $t_1 = 0$ gives the mean square value of $x(t_0)$:

$$R_x(t_0, 0) = E[x^2(t_0)] = \sigma_x^2(t_0) + m_x^2(t_0). \tag{16}$$

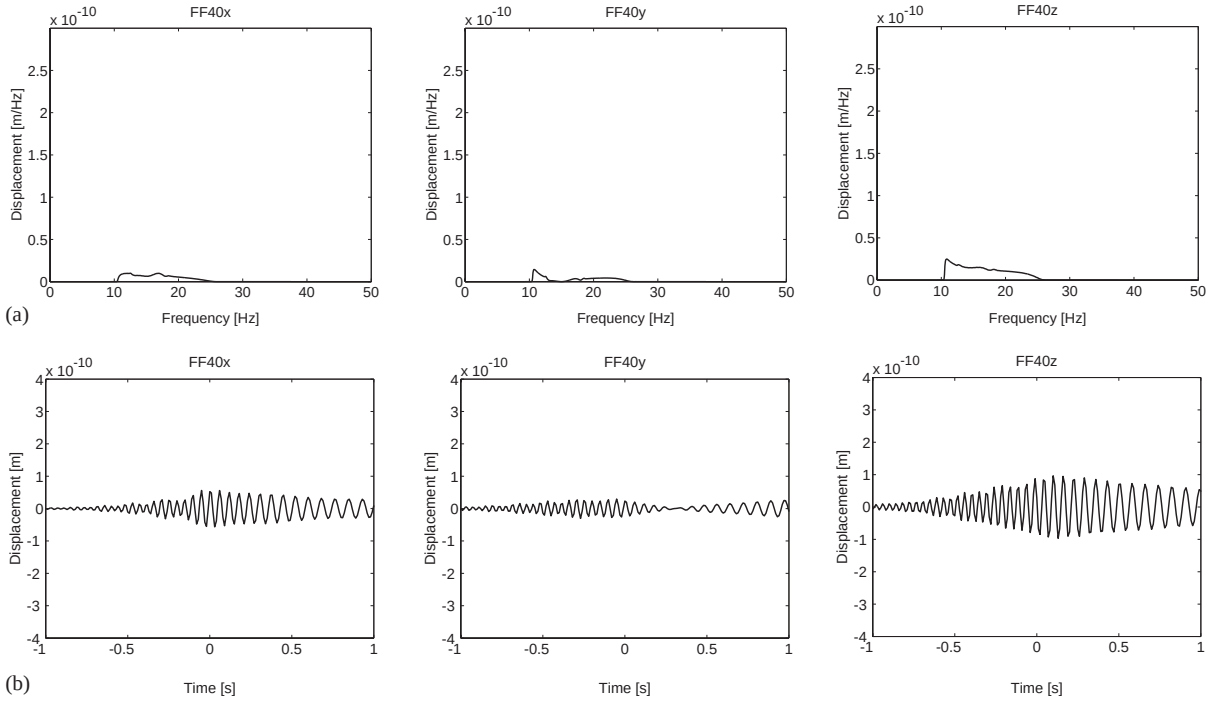

Fig. 5. (a) Frequency content and (b) time history of the freefield displacement at $x = 40$ m for a moving harmonic load with a frequency $\tilde{\omega}_S = 2\pi 15$ Hz and a speed $v = 60$ m/s.

For a random process $x(t)$ with a zero mean value $m_x(t_0)$, $R_x(t_0, 0)$ is equal to the square of the standard deviation $\sigma_x(t_0)$, or:

$$\sigma_x(t_0) = \sqrt{R_x(t_0, 0)}. \tag{17}$$

For a stationary random process $x(t)$, the standard deviation and the mean value are independent of the absolute time t_0.

The autocorrelation function $R_x(t_0, t_1)$ and the instantaneous spectral density $S_x(t_0, \omega_0)$ of the non-stationary random process $x(t)$ are a Fourier transform pair with respect to the dual variables t_1 and ω_0:

$$R_x(t_0, t_1) = \frac{1}{2\pi} \int_{-\infty}^{\infty} S_x(t_0, \omega_0) \exp(+\mathrm{i}\omega_0 t_1)\, \mathrm{d}\omega_0,$$
$$S_x(t_0, \omega_0) = \int_{-\infty}^{+\infty} R_x(t_0, t_1) \exp(-\mathrm{i}\omega_0 t_1)\, \mathrm{d}t_1. \tag{18}$$

The instantaneous spectral density is a measure of the frequency content of the random process $x(t)$ at a fixed time t_0. For a stationary process $x(t)$, the instantaneous spectral density does not vary with t_0. $S_x(t_0, \omega_0)$ is also referred to as the Wigner–Ville distribution.

The instantaneous spectral density function $S_x(t_0,\omega_0)$ and the double power spectral density $S_x(\omega_1,\omega_0)$ are a Fourier transform pair with respect to the dual variables t_0 and ω_1:

$$S_x(t_0,\omega_0)=\frac{1}{2\pi}\int_{-\infty}^{\infty}S_x(\omega_1,\omega_0)\exp(+\mathrm{i}\omega_1 t_0)\,\mathrm{d}\omega_1,$$
$$S_x(\omega_1,\omega_0)=\int_{-\infty}^{+\infty}S_x(t_0,\omega_0)\exp(-\mathrm{i}\omega_1 t_0)\,\mathrm{d}t_0. \tag{19}$$

The double power spectral density $S_x(\omega_1,\omega_0)$ is a measure of the variation of the instantaneous spectral density function $S_x(t_0,\omega_0)$ with respect to t_0. For a stationary random process $x(t)$, the double power spectral density $S_x(\omega_1,\omega_0)$ is zero for all ω_1 but $\omega_1=0$, where its value is undefined. Analogously, for a process where the statistical properties vary slowly, large values of $S_x(\omega_1,\omega_0)$ are concentrated at low circular frequencies ω_1.

For a real-valued random process $x(t)$, the following expression can be derived for the double power spectral density $S_x(\omega_1,\omega_0)$:

$$S_x(\omega_1,\omega_0)=E\left[\hat{x}^*\left(\omega_0-\frac{\omega_1}{2}\right)\hat{x}\left(\omega_0+\frac{\omega_1}{2}\right)\right] \tag{20}$$

where the superscript * denotes the complex conjugate. For an arbitrary real-valued non-stationary process, the local spectral density $S_x(-\omega_1,\omega_0)$ is equal to the complex conjugate $S_x^*(\omega_1,\omega_0)$. Under the same conditions, $S_x(\omega_1,-\omega_0)$ is equal to $S_x(\omega_1,\omega_0)$.

3.3. A set of arbitrary random moving loads

Consider a set of moving loads $\rho b_j(\mathbf{x},t)=\sum_{k=1}^{n},\delta(\mathbf{x}-\mathbf{x}_{Sk}(t))g_k(t)\delta_{zj}$ with a time-dependent position $\mathbf{x}_{Sk}(t)=\{x_S,y_k+vt,z_S\}^{\mathrm{T}}$ and a time history $g_k(t)$. The stationary random process $g_k(t)$ is characterized by the autocorrelation function $R_{g_k}(\tau)$ and the spectral density $S_{g_k}(\omega)$. $R_{g_{kl}}(\tau)$ and $S_{g_{kl}}(\omega)$ represent the cross-correlation and the cross-power spectral density of $g_k(t)$ and $g_l(t)$.

$S_{u_{ikl}}(\mathbf{x},\omega_1,\omega_0)$ denotes the cross-power spectral density of the soil's response at a point $\mathbf{x}=\{x,y,z\}^{\mathrm{T}}$ in the direction $\mathbf{e}_i$ for two random moving loads $g_k(t)$ and $g_l(t)$ and is calculated according to Eq. (20), where the frequency content of the response to a single axle load is computed by means of Eq. (12):

$$\begin{aligned}S_{u_{ikl}}(\mathbf{x},\omega_1,\omega_0)=E\Bigg[&\left\{\frac{1}{2\pi v}\int_{-\infty}^{+\infty}\hat{g}_k^*(\tilde{\omega})\tilde{h}_{zi}^*\left(x,\frac{\omega_0-(\omega_1/2)-\tilde{\omega}}{v},z,\omega_0-\frac{\omega_1}{2}\right)\right.\\&\left.\times\exp\left[+\mathrm{i}\left(\frac{\omega_0-(\omega_1/2)-\tilde{\omega}}{v}\right)(y-y_k)\right]\mathrm{d}\tilde{\omega}\right\}\\&\times\left\{\frac{1}{2\pi v}\int_{-\infty}^{+\infty}\hat{g}_l(\tilde{\omega}')\tilde{h}_{zi}\left(x,\frac{\omega_0+(\omega_1/2)-\tilde{\omega}'}{v},z,\omega_0+\frac{\omega_1}{2}\right)\right.\\&\left.\times\exp\left[-\mathrm{i}\left(\frac{\omega_0+(\omega_1/2)-\tilde{\omega}'}{v}\right)(y-y_l)\right]\mathrm{d}\tilde{\omega}'\right\}\Bigg].\end{aligned} \tag{21}$$

As the position of the load is known exactly, the expectation is restricted to the random character of the load:

$$S_{u_{ikl}}(\mathbf{x},\omega_1,\omega_0) = \frac{1}{4\pi^2 v^2}\int_{-\infty}^{+\infty}\int_{-\infty}^{+\infty} E[\hat{g}_k^*(\tilde{\omega})\hat{g}_l(\tilde{\omega}')] \times \tilde{h}_{zi}^*\left(x,\frac{\omega_0-(\omega_1/2)-\tilde{\omega}}{v},z,\omega_0-\frac{\omega_1}{2}\right) \times \exp\left[+\mathrm{i}\left(\frac{\omega_0-(\omega_1/2)-\tilde{\omega}}{v}\right)(y-y_k)\right] \times \tilde{h}_{zi}\left(x,\frac{\omega_0+(\omega_1/2)-\tilde{\omega}'}{v},z,\omega_0+\frac{\omega_1}{2}\right) \times \exp\left[-\mathrm{i}\left(\frac{\omega_0+(\omega_1/2)-\tilde{\omega}'}{v}\right)(y-y_l)\right]\mathrm{d}\tilde{\omega}\,\mathrm{d}\tilde{\omega}'. \tag{22}$$

For two stationary random processes $g_k(t)$ and $g_l(t)$, it can be shown that

$$E[\hat{g}_k^*(\tilde{\omega})\hat{g}_l(\tilde{\omega}')] = 2\pi\delta(\tilde{\omega}'-\tilde{\omega})S_{g_{kl}}(\tilde{\omega}'). \tag{23}$$

If this relation is introduced in Eq. (22), the following expression is obtained:

$$S_{u_{ikl}}(\mathbf{x},\omega_1,\omega_0) = \left[\frac{1}{2\pi v^2}\int_{-\infty}^{+\infty} S_{g_{kl}}(\tilde{\omega}) \times \tilde{h}_{zi}^*\left(x,\frac{\omega_0-(\omega_1/2)-\tilde{\omega}}{v},z,\omega_0-\frac{\omega_1}{2}\right) \times \tilde{h}_{zi}\left(x,\frac{\omega_0+(\omega_1/2)-\tilde{\omega}}{v},z,\omega_0+\frac{\omega_1}{2}\right) \times \exp\left[-\mathrm{i}\left(\frac{\omega_0-\tilde{\omega}}{v}\right)(y_k-y_l)\right]\mathrm{d}\tilde{\omega}\right] \times \exp\left[-\mathrm{i}\left(\frac{\omega_1}{2v}\right)(2y-y_k-y_l)\right]. \tag{24}$$

The total power spectral density $S_{u_i}(\mathbf{x},\omega_1,\omega_0)$ is equal to the superposition of the auto-power spectral densities $S_{u_{ikk}}(\mathbf{x},\omega_1,\omega_0)$ and the cross-power spectral densities $S_{u_{ikl}}(\mathbf{x},\omega_1,\omega_0)$:

$$S_{u_i}(\mathbf{x},\omega_1,\omega_0) = \sum_{k=1}^{n}\sum_{l=1}^{n} S_{u_{ikl}}(\mathbf{x},\omega_1,\omega_0). \tag{25}$$

The double power spectral density of the response is coupled to the PSD of the source through the wavenumber at which the transfer functions are evaluated.

In a similar way as in Eq. (12) for the computation of the deterministic response, the calculation of the double power spectral density of the response is based on the representation of the source–receiver transfer function in the frequency–wavenumber domain.

For a receiver at a position $\mathbf{x}_{kl} = \{x,(y_k+y_l)/2,z\}^{\mathrm{T}}$, the cross-power spectral density $S_{u_{ikl}}(\mathbf{x}_{kl},\omega_1,\omega_0)$ is equal to the bracketed integral in Eq. (24). This equation can therefore be rewritten as follows:

$$S_{u_{ikl}}(\mathbf{x},\omega_1,\omega_0) = S_{u_{ikl}}(\mathbf{x}_{kl},\omega_1,\omega_0)\exp\left[-\mathrm{i}\left(\frac{\omega_1}{2v}\right)(2y-y_k-y_l)\right]. \tag{26}$$

The instantaneous spectral density function is obtained as the inverse Fourier transform of $S_{u_{ikl}}(\mathbf{x}, \omega_1, \omega_0)$ with respect to the circular frequency ω_1:

$$S_{u_{ikl}}(\mathbf{x}, t_0, \omega_0) = \frac{1}{2\pi} \int_{-\infty}^{\infty} S_{u_{ikl}}(\mathbf{x}_{kl}, \omega_1, \omega_0) \times \exp\left[-\mathrm{i}\left(\frac{\omega_1}{2v}\right)(2y - y_k - y_l)\right] \exp(+\mathrm{i}\omega_1 t_0)\, \mathrm{d}\omega_1. \tag{27}$$

The exponential functions are collected as follows:

$$S_{u_{ikl}}(\mathbf{x}, t_0, \omega_0) = \frac{1}{2\pi} \int_{-\infty}^{\infty} S_{u_{ikl}}(\mathbf{x}_{kl}, \omega_1, \omega_0) \times \exp\left[+\mathrm{i}\omega_1 \left(t_0 - \frac{2y - y_k - y_l}{2v}\right)\right] \mathrm{d}\omega_1. \tag{28}$$

The term $(2y - y_k - y_l)/2v$ is a time shift applied on the instantaneous spectral density of the response at the point $\mathbf{x}_{kl}$:

$$S_{u_{ikl}}(\mathbf{x}, t_0, \omega_0) = S_{u_{ikl}}\left(\mathbf{x}_{kl}, t_0 - \frac{2y - y_k - y_l}{2v}, \omega_0\right). \tag{29}$$

3.4. A single random moving load

For a single random moving load, characterized by an autocorrelation $R_g(\tau)$ and a PSD $S_g(\omega)$, the double summation in Eq. (25) reduces to a single term and Eq. (24) can be further simplified:

$$S_{u_i}(\mathbf{x}, \omega_1, \omega_0) = \left[\frac{1}{2\pi v^2} \int_{-\infty}^{+\infty} S_g(\tilde{\omega}) \tilde{h}_{zi}^*\left(x, \frac{\omega_0 - (\omega_1/2) - \tilde{\omega}}{v}, z, \omega_0 - \frac{\omega_1}{2}\right) \times \tilde{h}_{zi}\left(x, \frac{\omega_0 + (\omega_1/2) - \tilde{\omega}}{v}, z, \omega_0 + \frac{\omega_1}{2}\right) \mathrm{d}\tilde{\omega}\right] \times \exp\left[-\mathrm{i}\left(\frac{\omega_1}{v}\right)(y - y_k)\right]. \tag{30}$$

For a receiver at $\mathbf{x}_k = \{x, y_k, z\}^{\mathrm{T}}$, the double power spectral density $S_{u_i}(\mathbf{x}_k, \omega_1, \omega_0)$ is equal to the bracketed integral, so that Eq. (30) can be rewritten as follows:

$$S_{u_i}(\mathbf{x}, \omega_1, \omega_0) = S_{u_i}(\mathbf{x}_k, \omega_1, \omega_0) \exp\left[-\mathrm{i}\left(\frac{\omega_1}{v}\right)(y - y_k)\right]. \tag{31}$$

In a similar way as for the cross-power spectral density for a set of random moving loads, the instantaneous spectral density at an arbitrary position $\mathbf{x}$ is calculated from the value at $\mathbf{x}_k$, applying a time shift $(y - y_k)/v$:

$$S_{u_i}(\mathbf{x}, t_0, \omega_0) = S_{u_i}\left(\mathbf{x}_k, t_0 - \frac{y - y_k}{v}, \omega_0\right). \tag{32}$$

3.5. A single random harmonic moving load

Consider a single moving harmonic load $g(t) = P\cos(\tilde{\omega}_S t + \phi)$ with a random phase angle ϕ that is uniformly distributed in the interval $[0, 2\pi]$. The autocorrelation function $R_g(\tau)$ is equal to $0.5P^2\cos(\tilde{\omega}_S\tau)$ and the power spectral density $S_g(\omega)$ equals $0.5\pi P^2[\delta(\omega - \tilde{\omega}_S) + \delta(\omega + \tilde{\omega}_S)]$ [19].

The double power spectral density $S_{u_i}(\mathbf{x}_k, \omega_1, \omega_0)$ is computed according to Eq. (30):

$$\begin{aligned} S_{u_i}(\mathbf{x}_k, \omega_1, \omega_0) = {} & \frac{P^2}{4v^2}\tilde{h}^*_{zi}\left(x, \frac{\omega_0 - (\omega_1/2) - \tilde{\omega}_S}{v}, z, \omega_0 - \frac{\omega_1}{2}\right) \\ & \times \tilde{h}_{zi}\left(x, \frac{\omega_0 + (\omega_1/2) - \tilde{\omega}_S}{v}, z, \omega_0 + \frac{\omega_1}{2}\right) \\ & + \frac{P^2}{4v^2}\tilde{h}^*_{zi}\left(x, \frac{\omega_0 - (\omega_1/2) + \tilde{\omega}_S}{v}, z, \omega_0 - \frac{\omega_1}{2}\right) \\ & \times \tilde{h}_{zi}\left(x, \frac{\omega_0 + (\omega_1/2) + \tilde{\omega}_S}{v}, z, \omega_0 + \frac{\omega_1}{2}\right). \end{aligned} \tag{33}$$

Comparison with Eq. (14) demonstrates that the first term on the right-hand side of this equation represents the product of the frequency content of the response at a circular frequency $\omega_0 - \omega_1/2$ and $\omega_0 + \omega_1/2$, respectively, due to a deterministic harmonic source at $\tilde{\omega}_S$. The second term in this equation represents the contribution from a harmonic source at $-\tilde{\omega}_S$.

In the previous examples, it has been shown that the response to a deterministic harmonic source at a circular frequency $\tilde{\omega}_S$ and with a speed v is mainly situated in the frequency band $[\tilde{\omega}_S/(1 + v/C_R), \tilde{\omega}_S/(1 - v/C_R)]$. As a result, the first term on the right-hand side of Eq. (33)

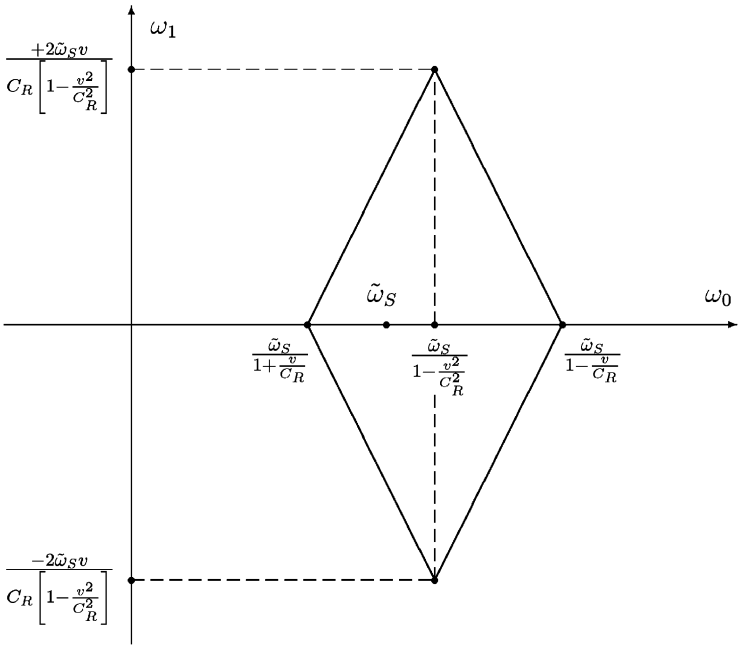

Fig. 6. The diamond-shaped area in the (ω_0, ω_1)-domain where inequalities (34) are met.

contributes significantly if $\omega_0 - \omega_1/2$ and $\omega_0 + \omega_1/2$ satisfy the following inequalities:

$$\frac{\tilde{\omega}_S}{(1+v/C_R)} \leqslant \omega_0 - \frac{\omega_1}{2} \leqslant \frac{\tilde{\omega}_S}{(1-v/C_R)} \quad \text{and} \quad \frac{\tilde{\omega}_S}{(1+v/C_R)} \leqslant \omega_0 + \frac{\omega_1}{2} \leqslant \frac{\tilde{\omega}_S}{(1-v/C_R)}, \tag{34}$$

which defines a diamond-shaped area in the (ω_0, ω_1)-domain (Fig. 6).

Analogously, the second term on the right-hand side of Eq. (33) determines a diamond-shaped area in the (ω_0, ω_1)-domain that is the mirrored shape of the area in Fig. 6. For the contribution of the P- and S-waves similar diamond shaped areas are found.

The foregoing discussion illustrates that the frequency content of the double power spectral density $S_{u_i}(\mathbf{x}_k, \omega_1, \omega_0)$ with respect to ω_0 is similar to the frequency content of the response in the deterministic case. The frequency content of $S_{u_i}(\mathbf{x}_k, \omega_1, \omega_0)$ with respect to ω_1 is situated at lower frequencies. This indicates that the variation of the instantaneous autocorrelation function with the absolute time t_0 is slower than the variation with the separation time t_1, which is due to the fact that the variation of the statistical properties of the response is slower than the variation of the deterministic signal.

3.6. Analytical example

When the presence of the road is neglected and the moving load is directly applied at the free surface of a homogeneous half-space, the contribution of the S-wave to the response at the free surface is estimated as [10]:

$$u_{si}(\mathbf{x}, t) \approx \frac{\delta_{zi}}{r_t^2} f\left(t - \frac{r_t}{C_s}\right), \tag{35}$$

where r_t denotes the distance $\|\mathbf{x} - \mathbf{x}_S(t)\|$ between the receiver and the moving source at the time t. In the following, it is assumed that the moving load is initially located at the origin of the Cartesian frame of reference, so that $\mathbf{x}_S(t) = \{0, vt, 0\}^{\mathrm{T}}$. The function f depends on the material properties of the half-space, on the receiver location $\mathbf{x}$ and on the time history of the moving load. As the latter is a random process, f represents a random process as well.

The local autocorrelation function $R_{u_{sz}}(\mathbf{x}, t_0, t_1)$ is defined by Eq. (15):

$$\begin{aligned} R_{u_{sz}}(\mathbf{x}, t_0, t_1) &= E\left[u_{sz}\left(\mathbf{x}, t_0 - \frac{t_1}{2}\right) u_{sz}\left(\mathbf{x}, t_0 + \frac{t_1}{2}\right)\right] \\ &\approx E\left[\frac{1}{r^2_{t_0+t_1/2}} f\left(t_0 + \frac{t_1}{2} - \frac{r_{t_0+t_1/2}}{C_s}\right) \frac{1}{r^2_{t_0-t_1/2}} f\left(t_0 - \frac{t_1}{2} - \frac{r_{t_0-t_1/2}}{C_s}\right)\right]. \end{aligned} \tag{36}$$

When the time history of the load is a fast oscillating function of the time t, it can be assumed that the variation of r_t with t is small and the radii $1/r_{t_0+t_1/2}$ and $1/r_{t_0-t_1/2}$ are approximately equal to $1/r_{t_0}$:

$$R_{u_{sz}}(\mathbf{x}, t_0, t_1) \approx \frac{1}{r^4_{t_0}} E\left[f\left(t_0 + \frac{t_1}{2} - \frac{r_{t_0+t_1/2}}{C_s}\right) f\left(t_0 - \frac{t_1}{2} - \frac{r_{t_0-t_1/2}}{C_s}\right)\right]. \tag{37}$$

Assuming that t_1 is small compared to t_0, the radius $r_{t_0+t_1/2}$ is approximated as

$$r_{t_0+t_1/2} = r_{t_0}\sqrt{1-\frac{vt_1(y-vt_0)}{r_{t_0}^2}} \approx r_{t_0}\left[1-\frac{vt_1(y-vt_0)}{2r_{t_0}^2}\right]. \tag{38}$$

Eq. (38) is used to approximate the local autocorrelation function in Eq. (37) as

$$R_{u_{sz}}(\mathbf{x},t_0,t_1) \approx \frac{1}{r_{t_0}^4} E\left[f\left(t_0+\frac{t_1}{2}-\frac{r_{t_0}\left[1-\frac{vt_1(y-vt_0)}{2r_{t_0}^2}\right]}{C_s}\right) \times f\left(t_0-\frac{t_1}{2}-\frac{r_{t_0}\left[1+\frac{vt_1(y-vt_0)}{2r_{t_0}^2}\right]}{C_s}\right)\right]. \tag{39}$$

The expected value in the right-hand side of Eq. (39) can be written as a function of the local autocorrelation function $R_f(t_0,t_1)$ of the random process f:

$$R_{u_{sz}}(\mathbf{x},t_0,t_1) \approx \frac{1}{r_{t_0}^4} R_f\left(t_0-\frac{r_{t_0}}{C_s}, t_1\left[1+\frac{v}{C_s}\frac{(y-vt_0)}{r_{t_0}}\right]\right). \tag{40}$$

The ratio $(y-vt_0)/r_{t_0}$ represents, at a time t_0, the cosine of the angle θ_{t_0} between the direction of propagation $\mathbf{e}_y$ and the line that connects the source and the receiver. Eq. (40) can therefore be rewritten as

$$R_{u_{sz}}(\mathbf{x},t_0,t_1) \approx \frac{1}{r_{t_0}^4} R_f\left(t_0-\frac{r_{t_0}}{C_s}, t_1\left[1+\frac{v\cos\theta_{t_0}}{C_s}\right]\right). \tag{41}$$

The local spectral density $S_{u_{sz}}(\mathbf{x},t_0,\omega_0)$ is obtained as the forward Fourier transform of $R_{u_{sz}}(\mathbf{x},t_0,t_1)$ with respect to t_1:

$$S_{u_{sz}}(\mathbf{x},t_0,\omega_0) \approx \frac{1}{r_{t_0}^4}\frac{C_s}{|C_s+v\cos\theta_{t_0}|} S_f\left(t_0-\frac{r_{t_0}}{C_s}, \omega_0\left[\frac{C_s}{C_s+v\cos\theta_{t_0}}\right]\right). \tag{42}$$

For a random harmonic load with a circular frequency $\tilde{\omega}_S$, the second argument of S_f is equal to $\tilde{\omega}_S$ and $\omega_0 = \tilde{\omega}_S(1+(v\cos\theta_{t_0}/C_s))$. The ratio $C_s/\cos\theta_{t_0}$ denotes the phase velocity C_{sy} of the S-waves in the y-direction at a time t_0. This relation can be compared to the exact relation $\omega = \tilde{\omega}_S/(1-v/C_{sy})$ as derived from the deterministic solution. For small velocities v with respect to C_s, both relations yield similar results. The difference between both expressions is due to the approximation in Eq. (38). These results indicate that the Doppler effect depends on the projection of the speed v on the direction between the source and the receiver.

The contribution of the P- and R-waves can be estimated in a similar way, replacing C_s in Eq. (42) by C_p or C_R. In the latter case, however, the geometric attenuation in Eqs. (41) and (42) is proportional to $1/r_{t_0}$ instead of $1/r_{t_0}^4$.

3.7. Numerical examples

In the following numerical examples, the non-stationary freefield response is computed for the case where a moving harmonic load $g(t) = \cos(\tilde{\omega}_S t + \phi)$ with a uniformly distributed random phase angle ϕ is applied to a road supported by a homogeneous half-space. The circular frequency $\tilde{\omega}_S$ of the harmonic load is equal to $2\pi 15$ rad/s and two source speeds $v = 20$ m/s and $v = 60$ m/s are considered.

Eq. (33) is used to compute the double power spectral density $S_{u_i}(\mathbf{x}, \omega_1, \omega_0)$ of the freefield response for a frequency f_0 upto 50 Hz, with $\Delta f_0 = 0.0488$ Hz ($N_0 = 1024$), corresponding to a period $T_1 = 20.48$ s and a time step $\Delta t_1 = 0.01$ s. The maximum value of f_1 is equal to 12.5 Hz, with $\Delta f_1 = 0.0488$ Hz ($N_1 = 256$), corresponding to a period $T_0 = 20.48$ s and a time step $\Delta t_0 = 0.04$ s.

Fig. 7a shows a contour plot of the double power spectral density $S_{u_i}(\mathbf{x}, \omega_0, \omega_1)$ of the freefield response at the soil's surface at $x = 8$ m. On these plots, it is indicated in which area of the (ω_0, ω_1)-domain the contribution of the R-, S- and P-waves is present. The contribution of the R-waves is bounded by points located at (13.1 Hz, 0), (15.3 Hz, 4.4 Hz) and (17.5 Hz, 0). The straight lines in the contour plots of the double power spectral density of the y- and z-component of the response correspond to the peaks that are observed in the frequency content of the response in the deterministic case (Fig. 2a).

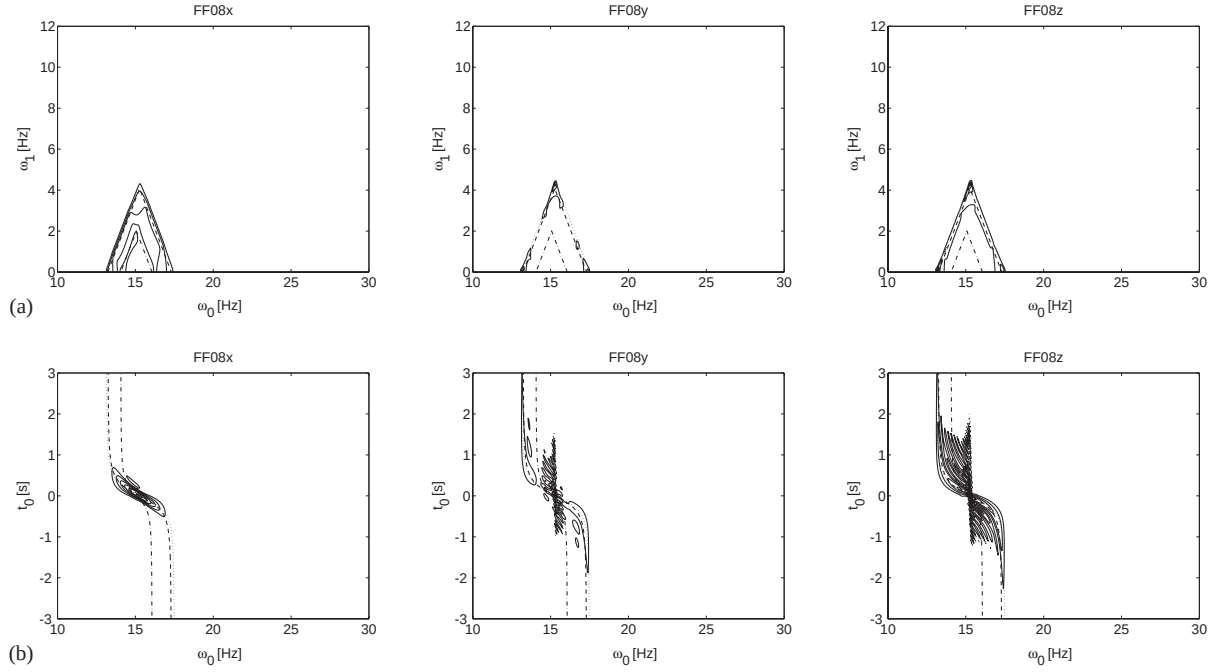

Fig. 7. (a) Double power spectral density $S_{u_i}(x, y_k, 0, \omega_0, \omega_1)$ and (b) instantaneous spectral density $S_{u_i}(x, y_k, 0, \omega_0, t_0)$ of the freefield response at $x = 8$ m for a random harmonic moving load with a frequency $\tilde{\omega}_S = 2\pi 15$ Hz and a speed $v = 20$ m/s. On both plots, the contribution of the R- (dotted line), S- (dashed line) and P-waves (dash–dotted line) is indicated.

Fig. 7b shows a contour plot of the instantaneous spectral density $S_{u_i}(\mathbf{x}, \omega_0, t_0)$ as a function of the absolute time t_0 and the circular frequency ω_0. The contribution of the S-, P- and R-waves has been indicated using Eq. (42), where the approximate relation $\omega_0 = \tilde{\omega}_S(1 + (v \cos \theta_{t_0}/C_s))$ is replaced by the exact relation $\omega_0 = \tilde{\omega}_S/(1 - (v \cos \theta_{t_0}/C_s))$.

The instantaneous spectral density shows how the frequency content of the random process varies with the absolute time t_0. At $t_0 \leqslant 0$, the source approaches and the frequency content with respect to ω_0 is situated at frequencies higher than $\tilde{\omega}_S$, whereas at $t_0 \geqslant 0$, the source recedes and the frequency content is situated at ω_0 lower than $\tilde{\omega}_S$. As in Fig. 2b, it is observed that the frequency shift for the P-waves is smaller than the shift for the R- and S-waves. This is due to the lower value of the ratio v/C_p with respect to v/C_s and v/C_R.

Fig. 8 shows similar results for the freefield response at 40 m from the centre of the road. The frequency shift with respect to t_0 now extends over a larger time due to the larger source–receiver distance.

Similar results have been calculated for the case where the source speed $v = 60$ m/s. The results for the corresponding deterministic case are shown in Figs. 4 and 5. The double power spectral density is calculated for a frequency f_0 upto 50 Hz, with $\Delta f_0 = 0.0977$ Hz ($N_0 = 512$), corresponding to a period $T_1 = 10.24$ s and a time step $\Delta t_1 = 0.01$ s. The maximum value of f_1

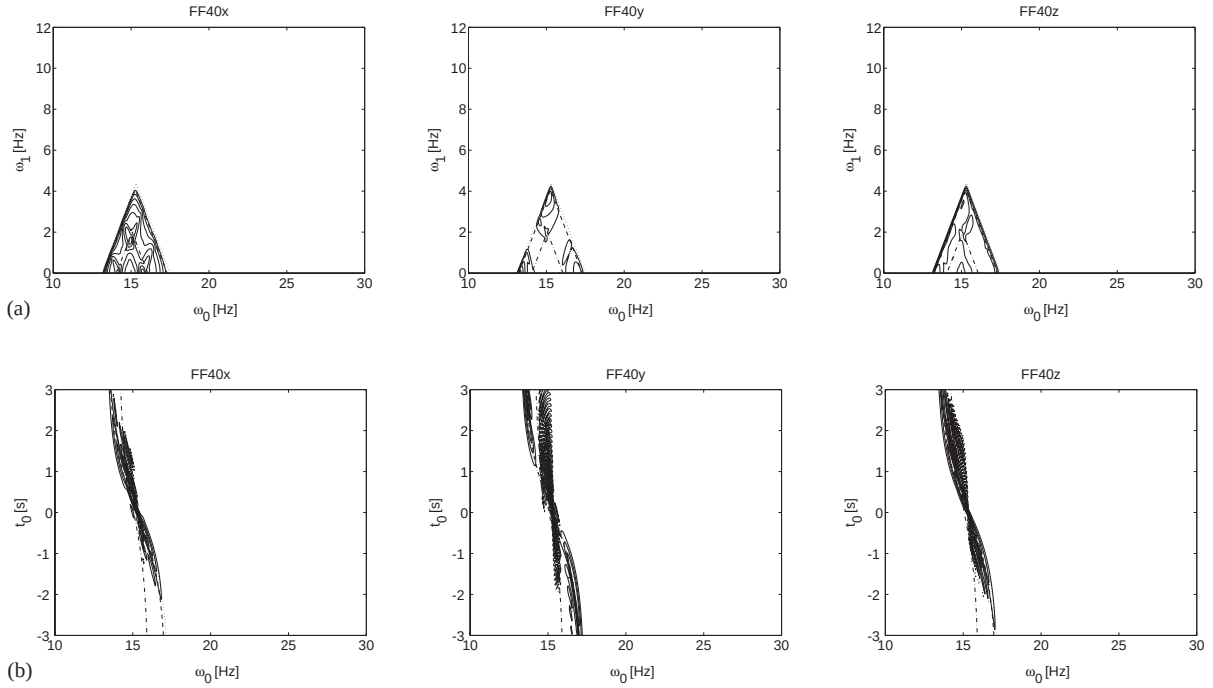

Fig. 8. (a) Double power spectral density $S_{u_i}(x, y_k, 0, \omega_0, \omega_1)$ and (b) instantaneous spectral density $S_{u_i}(x, y_k, 0, \omega_0, t_0)$ of the freefield response at $x = 40$ m for a random harmonic moving load with a frequency $\tilde{\omega}_S = 2\pi 15$ Hz and a speed $v = 20$ m/s. On both plots, the contribution of the R- (dotted line), S- (dashed line) and P-waves (dash–dotted line) is indicated.

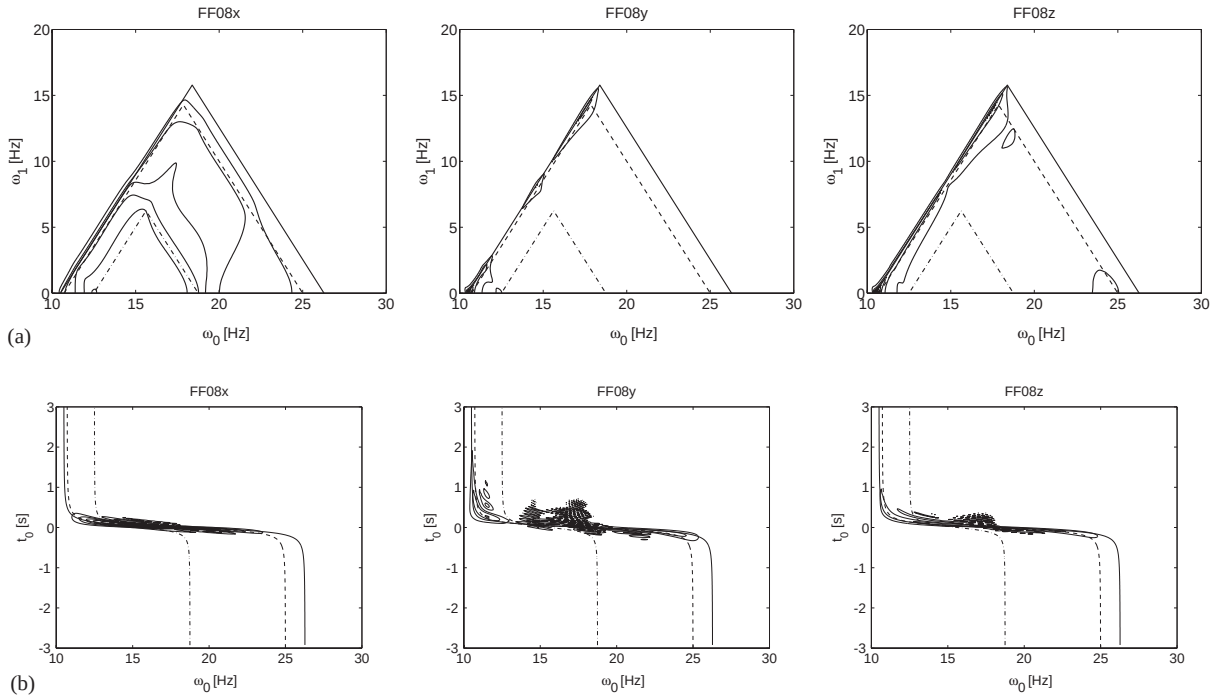

Fig. 9. (a) Double power spectral density $S_{u_i}(x, y_k, 0, \omega_0, \omega_1)$ and (b) instantaneous spectral density $S_{u_i}(x, y_k, 0, \omega_0, t_0)$ of the freefield response at $x = 8$ m for a random harmonic moving load with a frequency $\tilde{\omega}_S = 2\pi 15$ Hz and a speed $v = 60$ m/s. On both plots, the contribution of the R- (dotted line), S- (dashed line) and P-waves (dash–dotted line) is indicated.

is equal to 25 Hz, with $\Delta f_1 = 0.0977$ Hz ($N_1 = 256$), corresponding to a period $T_0 = 10.24$ s and a time step $\Delta t_0 = 0.02$ s.

The contribution of the R-wave in Fig. 9a is bounded by points located at (10.5 Hz, 0), (18.4 Hz, 15.8 Hz) and (26.3 Hz, 0). The range for the circular frequencies ω_1 and ω_0 in this area is now approximately three times larger than for the case where the source speed $v = 20$ m/s (Fig. 7a). In a similar way as in the deterministic case (Fig. 4a), the contribution at frequencies ω_0 lower than $\tilde{\omega}_S$ is larger than at frequencies higher than $\tilde{\omega}_S$. As the speed v of the source is three times larger than in the previous case, the frequency shift with respect to t_0 is much faster than in Fig. 7b.

Fig. 10 shows similar results at 40 m from the centre of the road. When the results in Fig. 10b are compared with the results in Figs. 8b and 9b, it is observed how the frequency shift with respect to t_0 depends on the distance x from the source line and the source speed v.

The instantaneous autocorrelation function $R_{u_i}(\mathbf{x}, t_0, t_1)$ is calculated as the inverse Fourier transform of the instantaneous spectral density $S_{u_i}(\mathbf{x}, t_0, \omega_0)$. The standard deviation $\sigma_{u_i}(\mathbf{x}, t_0)$ of the response is equal to $\sqrt{R_{u_i}(\mathbf{x}, t_0, t_1 = 0)}$.

Fig. 11 shows the standard deviation $\sigma_{u_i}(\mathbf{x}, t_0)$ of the response as a function of the absolute time t_0, together with the freefield response $u_{si}(\mathbf{x}, t)$ in the deterministic case (Fig. 2a), divided by a factor $\sqrt{2}$. In the stationary case where the load is applied at a fixed position, the response is a

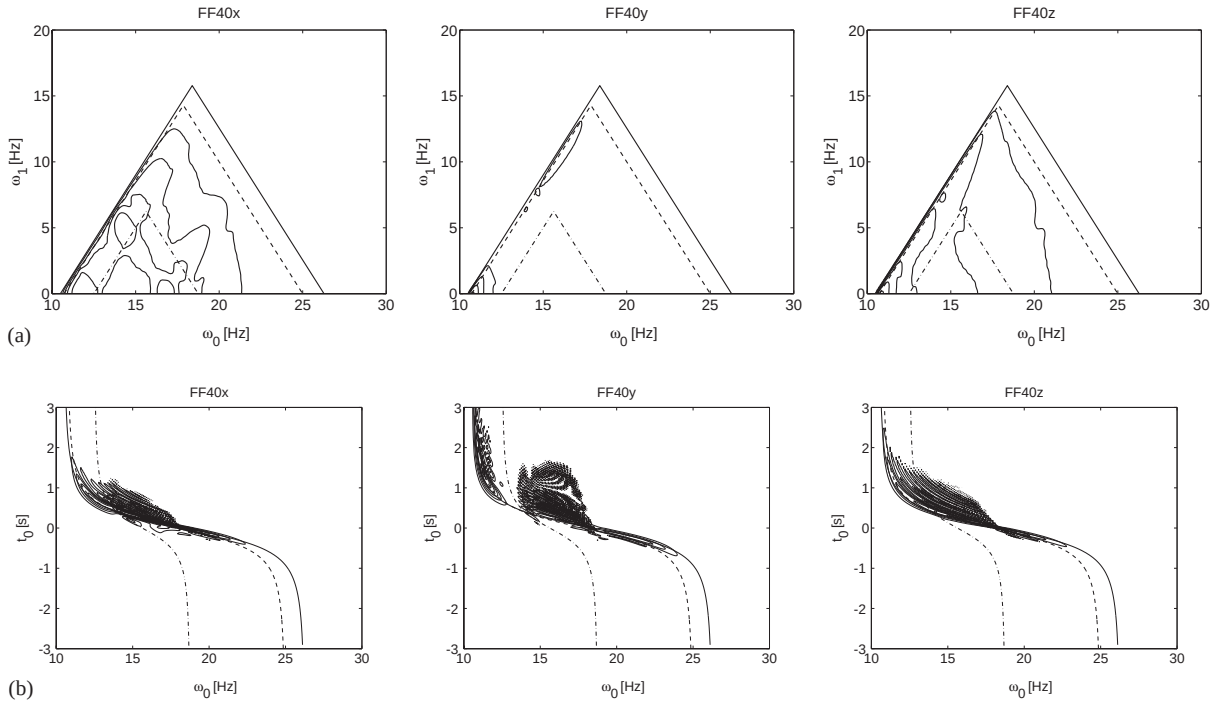

Fig. 10. (a) Double power spectral density $S_{u_i}(x, y_k, 0, \omega_0, \omega_1)$ and (b) instantaneous spectral density $S_{u_i}(x, y_k, 0, \omega_0, t_0)$ of the freefield response at $x = 40$ m for a random harmonic moving load with a frequency $\tilde{\omega}_S = 2\pi 15$ Hz and a speed $v = 60$ m/s. On both plots, the contribution of the R- (dotted line), S- (dashed line) and P-waves (dash–dotted line) is indicated.

purely harmonic signal at a circular frequency $\tilde{\omega}_S$. In this case, the standard deviation of the response is equal to the amplitude of the signal, divided by a factor $\sqrt{2}$. In the present case, the response is nearly harmonic and it is noticed in Fig. 11 how the relation between the standard deviation and the amplitude is nearly preserved.

The standard deviation shows a much smoother response and clearly follows the trend of the amplitude of the deterministic response. At a distance of 40 m from the source line (Fig. 11b), the standard deviation varies slowly with the absolute time t_0. The number of periods of the deterministic signal is high during the passage of the source. As the vehicle speed is low compared to the wave velocities in the soil, the freefield response mainly depends on the distance between the source and the receiver and the source can be assumed to be applied at a fixed position. In this case, a stationary stochastic method can be used to predict the freefield response.

Fig. 12 shows similar results for the case where the source speed $v = 60$ m/s. Comparison with the results presented in Fig. 11 shows that the peak amplitude of the response is approximately the same for both source speeds. This observation confirms that, for low speeds v with respect to the wave velocities in the soil, the response mainly depends on the source–receiver distance. The stochastic method clearly provides a useful tool for the prediction of the envelope of the deterministic response.

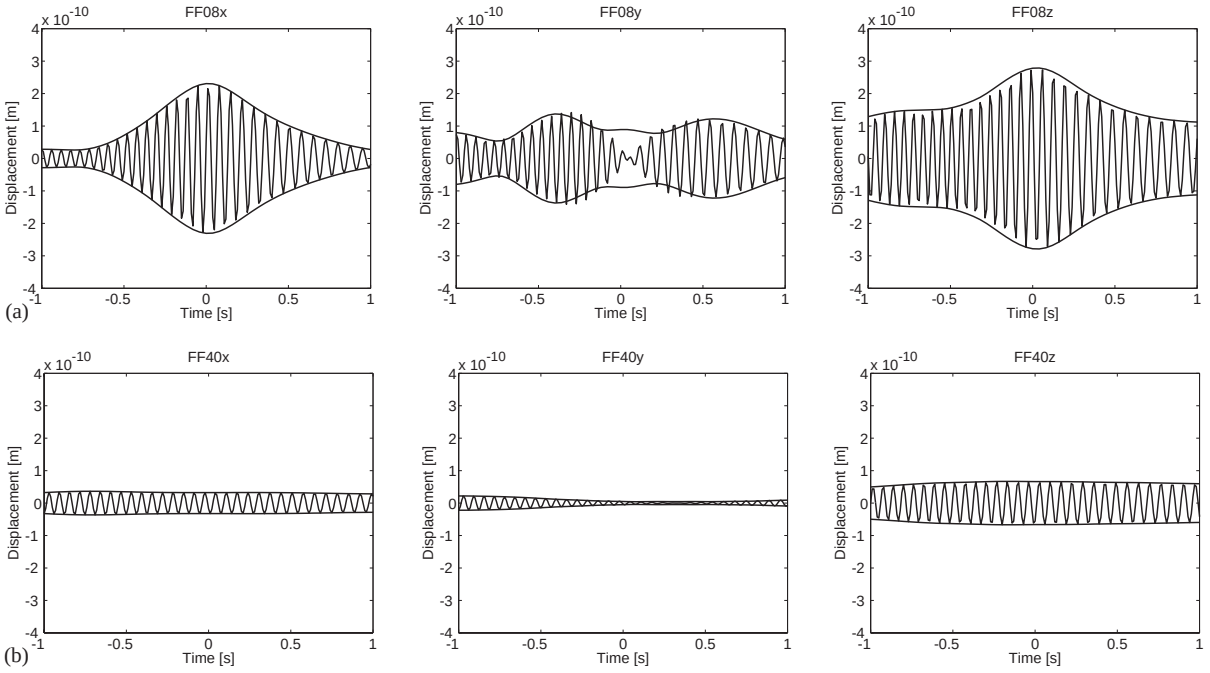

Fig. 11. The standard deviation $\sigma_{u_i}(x, y_k, 0, t_0)$ of the freefield response at (a) $x = 8$ m and (b) $x = 40$ m for a random harmonic moving load with a frequency $\tilde{\omega}_S = 2\pi$ 15 rad/s and a speed $v = 20$ m/s. On these graphs, the deterministic freefield response $u_{si}(x, y_k, 0, t)/\sqrt{2}$ is also shown.

4. Conclusions

In this paper, the Wigner–Ville method has been applied to characterize the non-stationary statistical characteristics of the response at a fixed point in the freefield for a moving load with a random amplitude. The main advantage of the presented solution procedure is that it allows for a direct calculation of the time-dependent statistical properties of the response. In this way, a calculation of the statistical properties by a large number of deterministic calculations is avoided.

The solution is based on the known deterministic results in the case where the problem geometry is invariant in the direction of the moving source. A key ingredient in this solution procedure is the transfer function between the source and the receiver, that represents the freefield response for an impulse load at a fixed position along the path of the moving source.

The stochastic method is illustrated for the case of a moving harmonic load with a random phase shift. The freefield response is calculated for two points in the freefield and two source speeds. The Wigner–Ville distribution $S_x(t_0, \omega_0)$ shows how the frequency content of the response changes during the passage of the moving source and illustrates the Doppler effect. The calculation of the time-dependent standard deviation of the response demonstrates how the method can be employed to predict the freefield vibration levels.

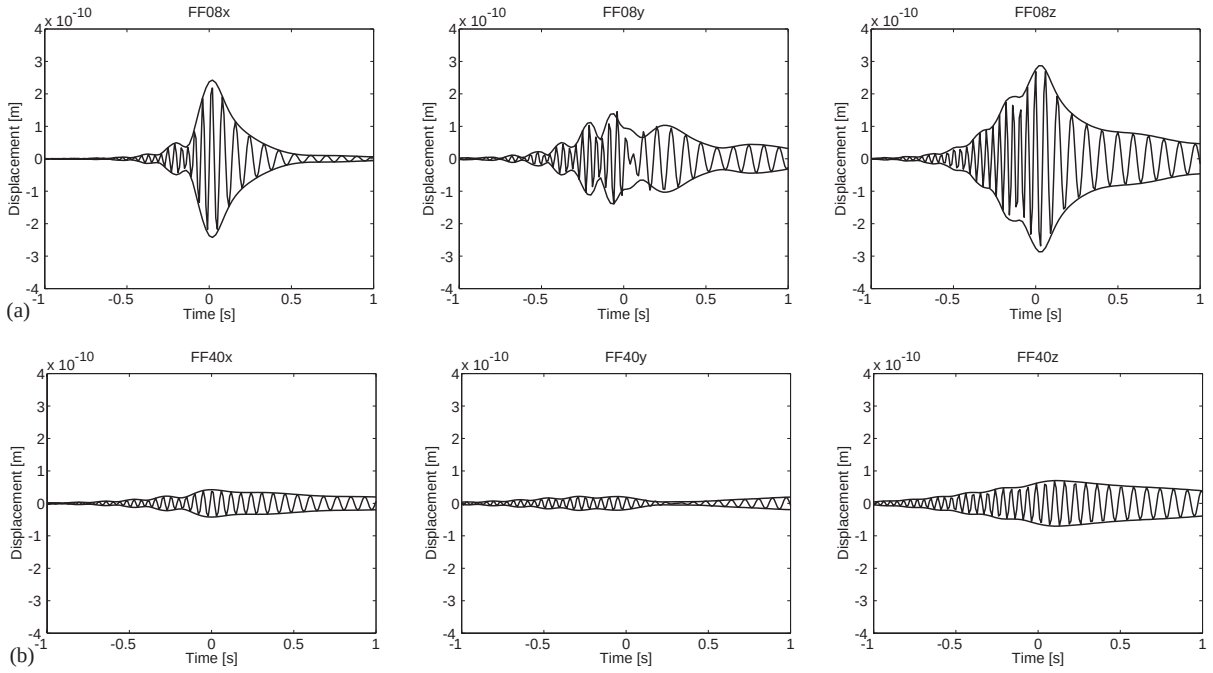

Fig. 12. The standard deviation $\sigma_{u_i}(x, y_k, 0, t_0)$ of the freefield response at (a) $x = 8$ m and (b) $x = 40$ m for a random harmonic moving load with a frequency $\tilde{\omega}_S = 2\pi$ 15 rad/s and a speed $v = 60$ m/s. On these graphs, the deterministic freefield response $u_{si}(x, y_k, 0, t)/\sqrt{2}$ is also shown.

Numerical results indicate that, in the case where the ratio x/v of the receiver distance x and the speed v is large with respect to the dominant period $T = 2\pi/\omega_S$ of the source, a deterministic analysis can be used to estimate the freefield vibration levels. If the response mainly depends on the source–receiver distance, the contact point between the vehicle and the road can be assumed to be fixed and a stationary stochastic analysis becomes applicable. The non-stationary method is therefore particularly useful in the case where the distance from the source line is small and the source speed is high.

Acknowledgements

The results presented in this paper have been obtained within the frame of the exchange project C98.001 between K.U. Leuven and Ecole Centrale de Paris. The support of both the Flemish Community and the CNRS is gratefully acknowledged.

The numerical model for the prediction of the freefield vibrations induced by road traffic has been developed within the frame of the research project MD/01/040 ''The study of determining factors for traffic induced vibrations in buildings''. This research project is supported by the Prime Minister's Services of the Belgian Federal Office for Scientific, Technical and Cultural Affairs and is part of the Sustainable Mobility programme.

The model has been further elaborated for the prediction of railway traffic induced vibrations within the frame of the STWW project IWT 000152 "Traffic induced vibrations in buildings", supported by the Flemish Community.

References

[1] R.G. Payton, An application of the dynamic Betti–Rayleigh reciprocal theorem to moving point loads in elastic media, *Quarterly of Applied Mathematics* 21 (4) (1964) 299–313.
[2] L. Frýba, *Vibration of Solids and Structures Under Moving Loads*, 3rd Edition, Thomas Telford, London, UK, 1999.
[3] G. Müller, Bewegter Streifenlast auf dem elastisch-isotropen Halbraum, *Acustica* 72 (1990) 47–53.
[4] G. Müller, H. Huber, Dynamische Bodeansprachungen infolgte bewegter Lasten, *Bauingenieur* 66 (1991) 375–380.
[5] F.C.P. de Barros, J.E. Luco, Moving Green's functions for a layered visco-elastic half-space, Technical Report, Department of Applied Mechanics and Engineering Sciences of the University of California, La Jolla, 1992.
[6] F.C.P. de Barros, J.E. Luco, Response of a layered viscoelastic half-space to a moving point load, *Wave Motion* 19 (1994) 189–210.
[7] H. Grundmann, M. Lieb, E. Trommer, The response of a layered half-space to traffic loads moving along its surface, *Archive of Applied Mechanics* 69 (1999) 55–67.
[8] D. Aubry, D. Clouteau, G. Bonnet, Modelling of wave propagation due to fixed or mobile dynamic sources, in: N. Chouw, G. Schmid (Eds.), *Workshop Wave '94, Wave propagation and Reduction of Vibrations*, Rühr University, Bochum, Germany, December 1994, pp. 109–121.
[9] D. Clouteau, MISS Revision 2.1, Notice Utilisateur, Laboratoire de Mécanique des Sols, Structures et Matériaux, Ecole Centrale de Paris, 1993.
[10] D. Clouteau, G. Degrande, G. Lombaert, Numerical modelling of traffic induced vibrations, *Meccanica* 36 (4) (2001) 401–420.
[11] M.S.A. Hardy, The generation of waves in infinite structures by moving harmonic loads, *Journal of Sound and Vibration* 180 (4) (1995) 637–644.
[12] C. Madshus, A.M. Kaynia, High-speed railway lines on soft ground: dynamic behaviour at critical train speed, *Journal of Sound and Vibration* 231 (3) (2000) 689–701.
[13] G. Degrande, G. Lombaert, An efficient formulation of Krylov's prediction model for train induced vibrations based on the dynamic reciprocity theorem, *Journal of the Acoustical Society of America* 110 (3) (2001) 1379–1390.
[14] C.J. Dodds, J.D. Robson, The description of road surface roughness, *Journal of Sound and Vibration* 31 (2) (1973) 175–183.
[15] ISO8608. *Mechanical vibration, road surface profiles*, Reporting of measured data, 1991.
[16] H. Hao, T.C. Ang, Analytical modelling of traffic-induced ground vibrations, *Journal of the Engineering Mechanics Division, Proceedings of the American Society of Chemical Engineers* 124 (8) (1998) 921–928.
[17] H.E.M. Hunt, Stochastic modelling of traffic-induced ground vibration, *Journal of Sound and Vibration* 144 (1) (1991) 53–70.
[18] L. Sun, B.S. Greenberg, Dynamic response of linear systems to moving stochastic sources, *Journal of Sound and Vibration* 229 (4) (2000) 957–972.
[19] D.E. Newland, *An Introduction to Random Vibrations, Spectral & Wavelet Analysis*, Longman Scientific & Technical, Essex, UK, 1994.
[20] G. Lombaert, G. Degrande, D. Clouteau, Deterministic and stochastic modelling of freefield traffic induced vibrations, in: P. Pereira, V. Miranda (Eds.), *International Symposium on the Environmental Impact of Road Pavement Unevenness*, Porto, Portugal, March 1999, pp. 163–176.
[21] G. Lombaert, G. Degrande, D. Clouteau, Numerical modelling of freefield traffic induced vibrations, *Soil Dynamics and Earthquake Engineering* 19 (7) (2000) 473–488.
[22] G. Lombaert, S. François, G. Degrande, J. Kogut, Validation of a numerical model for railway induced vibrations, in: *Proceedings of the Sixth National Congress on Theoretical and Applied Mechanics*, Ghent, Belgium, May 2003.

[23] J. Kogut, G. Lombaert, S. François, G. Degrande, W. Haegeman, L. Karl, High speed train induced vibrations: in situ measurements and numerical modelling, in: *Proceedings of the 10th International Congress on Sound and Vibration*, Stockholm, Sweden, July 2003, pp. 1689–1696 (CD-ROM).
[24] J. Kogut, G. Degrande, G. Lombaert, L. Pyl, L. Karl, W. Haegeman, Measurements and numerical prediction of high speed train vibrations, in: *Fifth International Conference on Case Histories in Geotechnical Engineering*, New York, NY, April 2004.
[25] G. Lombaert, G. Degrande, Experimental validation of a numerical prediction model for freefield traffic induced vibrations by in situ experiments, *Soil Dynamics and Earthquake Engineering* 21 (6) (2001) 485–497.
[26] G. Lombaert, G. Degrande, The experimental validation of a numerical model for the prediction of the vibrations in the freefield produced by road traffic, *Journal of Sound and Vibration* 262 (2003) 309–331.
[27] F.C.P. de Barros, J.E. Luco, Moving Green's functions for a layered visco-elastic halfspace, Technical Report, Department of Applied Mechanics and Engineering Sciences, University of California, San Diego, La Jolla, California, May, 1992.
[28] E. Kausel, J.M. Roësset, Stiffness matrices for layered soils, *Bulletin of the Seismological Society of America* 71 (6) (1981) 1743–1761.
[29] J.E. Luco, R.J. Apsel, On the Green's functions for a layered half-space. Part I, *Bulletin of the Seismological Society of America* 4 (1983) 909–929.
[30] G. Lombaert, Development and Experimental Validation of a Numerical Model for the Free Field Vibrations Induced by Road Traffic. Ph.D. Thesis, Department of Civil Engineering, Katholieke Universiteit Leuven, 2001.
[31] R.J. Apsel, J.E. Luco, On the Green's functions for a layered half-space. Part II, *Bulletin of the Seismological Society of America* 73 (1983) 931–951.
[32] G. Degrande, G. De Roeck, P. Van den Broeck, D. Smeulders, Application of a direct stiffness method to wave propagation in multiphase poroelastic media, *Meccanica* 32 (3) (1997) 205–214.
[33] G. Degrande, G. De Roeck, P. Van den Broeck, D. Smeulders, Wave propagation in layered dry, saturated and unsaturated poroelastic media, *International Journal of Solids and Structures* 35 (34–35) (1998) 4753–4778 (Poroelasticity Maurice A. Biot memorial issue).
[34] E.P. Wigner, On the quantum correction for thermodynamic equilibrium, *Physical Review* 40 (1932) 749–759.
[35] J. Ville, Théorie et applications de la notion de signal analytique, *Cables et Transmission* 2 (1948) 61–74.